Available online at www.sciencedirect.com
SCIENCE DIRECT®
Journal of Solid State Chemistry 176 (2003) 594–608
JOURNAL OF SOLID STATE CHEMISTRY
http://elsevier.com/locate/jssc

Electronic band structures and physical properties of $ALnTe_4$ and ALn_3Te_8 compounds (A = alkali metal; Ln = lanthanoid)

Klaus Stöwe*

Inorganic and Analytical Chemistry, Saarland University, FR 8.14, P.O. Box 15 11 50, 66041 Saarbruecken, Saarland, Germany

Received 14 February 2003; received in revised form 3 June 2003; accepted 10 June 2003

Abstract

We report about the LMTO-ASA band structure, ELF and COHP calculations for a number of alkali metal rare earth tellurides of the formulas $ALnTe_4$ (A= K, Rb, Cs and Ln= Pr, Nd, Gd) and KLn_3Te_8 (Ln= Pr, Nd) to point out structure-properties relations. The $ALnTe_4$ compounds crystallize in the $KCeSe_4$ structure type with Te ions arranged in the form of $4.3^2.4.3$ nets, in which interatomic homonuclear distances indicate an arrangement of isolated dumbbells. This could be verified by the COHP and ELF calculations, both of which revealed isolated $[Te_2]$ units. But in contrast to the ionic formulation as A^+Ln^{3+} $([Te_2]^{2-})_2$, which can be deduced from this observation, the band structure calculations for $KPrTe_4$, $KNdTe_4$, $RbNdTe_4$ and $CsNdTe_4$ reveal metallic conductivity. This behavior was verified for $KNdTe_4$ by resistivity measurements performed by a standard four-probe technique. We explain these results by an incomplete carryover of electrons from the rare earth cation onto tellurium due to covalent bonding leaving parts of the Te–Te $pp\pi^*$ antibonding states unoccupied. On the other hand the calculations suggest insulating behavior for $KGdTe_4$ resulting from a complete filling of the Te–Te $pp\pi^*$ antibonding states due to the increased stability of the half filled $4f$ shell. The ALn_3Te_8 compounds crystallize in the KNd_3Te_8 structure type, a distorted addition-defect variant of the $NdTe_3$ type with 4^4 Te nets. As polyanionic fragments L-shaped $[Te_3]^{2-}$ and infinite zig-zag chains $^1_\infty[Te_4]^{4-}$ are observed (with interatomic homonuclear distances in the range 2.82–3.00 Å), which are separated from each other by distances in the range 3.27–3.49 Å. Again COHP calculations made evident that these latter interactions are secondary. Within the infinite zig-zag chains $^1_\infty[Te_4]^{4-}$ the Te ions at the corners of the chain have a higher negative charge than the linear coordinated ones in the middle. KPr_3Te_8 and KNd_3Te_8 are semiconductors, verified for the latter by resistivity measurements.

Keywords: Alkali metal rare earth tellurides; Structure-properties relations; Magnetic properties; Resistivity; Electronic band structure calculations; Crystal orbital hamiltonian population COHP; Electron localization function ELF

1. Introduction

Understanding of measured physical properties of a compound is not possible without knowledge of the crystal structure. On the other hand it is not possible to compute physical properties of substances without receipt of structural information. So the structure is the interconnecting link between the design of a new compound and its practical application in material sciences. In many cases we think that we are able to predict properties from general concepts on the basis of the structure information alone, if the phases obey the simple valence rules, e.g., of Grimm and Sommerfeld, or Zintl, Klemm and Bussmann or of Mooser, Pearson, Kjekshus and Hulliger. But we should always keep in mind that the compounds are not able to resist against our attempts to describe them, as already stated by Schäfer [1]. In polytellurides we often fail to apply the common concepts and subsequently in many cases unforseen properties are measured. For example the compound $LaTe_2$ is a metallic conductor despite of the fact that in the crystal structure—a distortion variant of the anti-Fe_2As or Cu_2Sb type—only dumbbells of Te ions are observed [2]. According to von Schnering [3] the importance of a description can be measured to the extent to which the connection between stoichiometry (i.e. valence electron count), structure (i.e. electron distribution) and properties (like color, conductivity, magnetism, reactivity, etc.) can be represented.

*Fax: +49-681-3024233.
E-mail address: k.stoewe@mx.uni-saarland.de.

0022-4596/$ - see front matter © 2003 Elsevier Inc. All rights reserved.
doi:10.1016/S0022-4596(03)00345-1

In the past we characterized the crystal structures of a number of polytellurides with different stoichiometries such as $ALnTe_4$ (A = alkali metal, Ln = lanthanoid) [4,5] or ALn_3Te_8 [6]. With this contribution we want to enlighten the physical properties of these compounds and initiate the first step to describe them with the help of quantum mechanical band structure calculations.

1.1. Crystal structures

All compounds of the type $ALnTe_4$ crystallize in the $KCeSe_4$ structure type [7]. This structure type can be described as a layer structure with Te sheets in the form of $4.3^2.4.3$ nets. In these Te nets, common edges of neighboring triangles ($.3^2.$) reveal Te–Te distances of 2.775–2.780 Å, i.e. in the range of typical single-bond distances. The compound diphenyl ditelluride may serve as a reference, in which the Te–Te distance is 2.76 Å [8]. On the other hand the distances between the dumbbells are 3.719–3.781 Å, i.e. well above the range of secondary Te–Te interactions (3.2–3.5 Å). Between the Te layers cationic layers of A and Ln in the form of 4^4 nets are inserted and a layer sequence of 'A Te Ln Te′, A' in the [001] direction is observed. The two Te nets, Te and Te′, are rotated against each other by 90°. The vertices of the square nets coincide in a projection along [001] with the centers of the squares within the $4.3^2.4.3$ nets, so that the coordination polyhedra for both A and Ln are square antiprisms (CN = 8). By the 90° rotation the dumbbells are staggered crosswise along [001] forming rods. In Fig. 1 a projection of the structure along [001] is depicted.

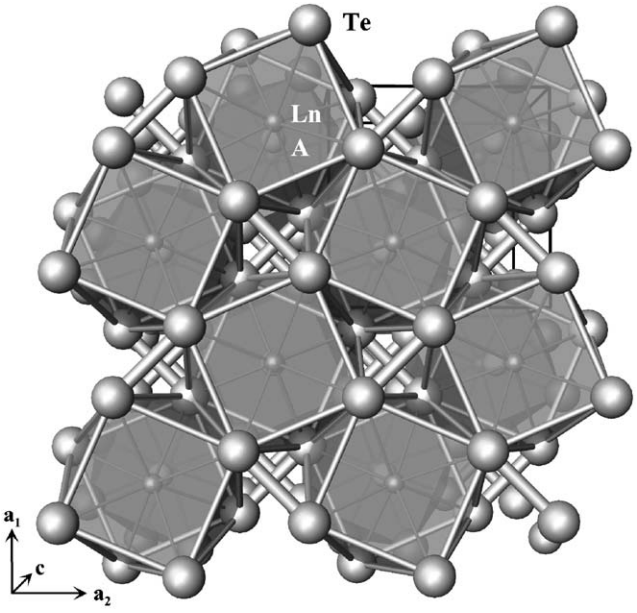

Fig. 1. Crystal structure of the $ALnQ_4$ compounds (A= K, Rb, Cs and Ln = Pr, Nd, Gd) in a projection along [001].

Sticking closer to the interatomic distances, it is to be observed that these can be interpreted largely by geometrical arguments [5]. A linear relation between the Ln^{3+} radii and the Ln–Te distances is observed with negligible secondary effects of the alkali metal cations. On the contrary the secondary effects of Ln^{3+} are more pronounced for the $A-Te$ distances, which additionally show the expected spread due to radii differences between K^+ and Rb^+ of ca. 0.1 Å. Among the homonuclear anion distances two types of distances are to be considered, intra and interdumbbell distances. Due to the tetragonal symmetry of the compounds and the special site symmetry of the Te positions in all only two different Te–Te distances are to be distinguished. Among the tellurides of this structure type the intradumbbell distances are identical within the experimental errors (see above), and show no variation with cation radii. This is not true for the interdumbbell distances. Here, effects of the Ln^{3+} as well as the A^+ radii are observed. Because of the small variation width of the intradumbbell distance it is to be supposed that an ionic formulation of the $ALnTe_4$ compounds of this structure type as $\{A^+Ln^{3+}([Te_2]^{2-})_2\}$ should be adequate.

The Te atoms are arranged in the ALn_3Te_8 compounds not in the form of $4.3^2.4.3$ nets, but instead in the form of distorted defect square or 4^4 nets. In their 'simplest' form they are crystallizing isotypic to KNd_3Te_8 [9], a structure type, which can be described as a defect-addition variant of the $NdTe_3$ type [10]. The structure relations between these two types can be summarized by a group-subgroup relation in the form of a *Bärnighausen* family tree [11]. KNd_3Te_8 crystallizes monoclinic in space group $P12_1/a1$ [9], but here we use the standard setting proposed for KPr_3Te_8 in space group $P12_1/c1$ [6].

The $NdTe_3$ structure type is related topologically to the anti-Fe_2As or anti-Cu_2Sb type, which may be regarded as the idealized basis structure of the LnQ_2 (Q= S, Se, Te) compounds. This latter type is usually considered as a tetragonal layer structure with planar four-coordinate square or 4^4 lattices of Q^- interlayered with sheets of distorted cubes consisting of Ln^{3+} and Q^{2-}. This latter cubic motif is a distorted form of that found for the rock-salt monochalcogenides. In the $NdTe_3$ type LnQ_3 compounds an additional square sheet is inserted between the distorted rock-salt blocks, so that a van der Waals gap results combined with a typical crystal habit of the layered crystals. This is schematically depicted in the middle part of Fig. 2. In the ALn_3Q_8 type some of the Te in the square nets are removed in favor of additional alkali atoms within the van der Waals gap (Fig. 2 right side): by this the formula changes from Ln_3Q_9 to ALn_3Q_8. Regarding the coordination environment of the cations the following is observed: the Ln^{3+} cations in the $NdTe_3$ structure type are coordinated nine-fold in the form of a monocapped

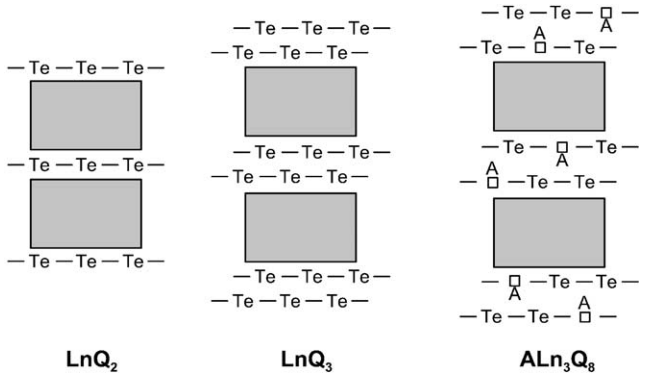

Fig. 2. Schematic representation of the structural relationships between compounds of formula type LnQ_2 (anti-Fe_2As or Cu_2Sb type), LnQ_3 ($NdTe_3$ type) and ALn_3Q_8 (KNd_3Te_8 type); in gray: distorted rock-salt blocks.

tetragonal anti-prism. Due to vacancies within the polytelluric layers, in the ALn_3Q_8 type now three crystallographically different rare earth atomic positions are to be distinguished: for two, the coordination number is reduced to eight and the coordination polyhedra are two-fold capped trigonal prisms instead of mono-capped tetragonal anti-prisms. For the third rare earth ion the coordination number and polyhedron is preserved. On the other hand the originally tetragonal planar coordination of the depleted Te atoms within the 4^4 nets changes due to the shift of atomic position into a distorted quadratic anti-prismatic environment of the alkali ions, as can be seen from Fig. 3. Formally the Te ions in the quadratic layers of the LnQ_3 type have a charge of -0.5. Due to the exchange of Te by A ions, each Te of the remaining ones gets a higher charge resulting in a distortion of square net into quasi-molecular fragments. Two different fragments are to be distinguished from considerations of interatomic distances: L-shaped triatomic units $[Te_3]^{2-}$ and infinite zig-zag chains $^1_\infty[Te_4]^{4-}$ running in the [001] direction. As depicted in Fig. 3, in the [010] direction these infinite chains alternate within one layer with rows of $[Te_3]^{2-}$ pairs. With interatomic distances of 2.83 Å, which is exactly the distance within the helical chains in elemental tellurium [12], and an angle of 99.1° (both data taken from KPr_3Te_8 [6]) a close relationship of the $[Te_3]^{2-}$ units to those observed in the alkali metal sesquitellurides, as, e.g. K_2Te_3 (2.80 and 2.81 Å, ∢104.4° [13]), is given. But in contrast to the alkali metal sesquitellurides the L-shaped $[Te_3]^{2-}$ units are not completely isolated: the next nearest-neighbor distance to the zig-zag chains being 3.27 Å, the question has to be solved, as to whether these distances are reflecting relevant interactions, which have to be taken into consideration in the formal charge distribution. Within the zig-zag chains $^1_\infty[Te_4]^{4-}$ there is only a slight interatomic distance alternation of 2.98 and 3.00 Å. The corresponding angles are 179.6 (at Te(5)) and 97.6° (at Te(4)) also indicating an alternation of linear and bent Te ions within the infinite zig-zag chains (see Fig. 3). This unit is unique insofar as it is not observed in any other compound with polytelluric fragments. Not as infinite chains, but as internally closed in the form of a ring a similar bonding situation is found in $NdTe_{1.89}$ with eight-membered rings [14]. Other still outstanding questions concerning the KNd_3Te_8 structure type are the formal charge distribution within the zig-zag chains of $(A^+)_2$ $(Ln^{3+})_6$ $(Te^{2-})_6$ $([Te_3]^{2-})_2$ $^1_\infty[Te_4]^{4-}$, the conductivity characteristics of the compounds of this structure type and the possibility of charge density waves within the infinite chains resulting in super-structure reflections as observed for KNd_3Te_3 in electron diffraction studies [9]. Concerning the last point there is an argument against a charge density wave coming from the observation of super-structure reflections due to different polytypes of the KNd_3Te_8 type. These polytypes were observed for KNd_3Te_8 itself and other compounds of this family. Finally these questions can only be solved by quantum mechanical calculations, the results of these being reported in this contribution.

2. Experimental

2.1. Synthesis

Syntheses of the title compounds were performed by a flux technique [15] using the alkali metal sesquitellurides A_2Te_3 as a reactant and flux medium. Details can be found in Refs. [4–6]. In contrast to the procedure described in Ref. [6] a reactant ratio of $3A_2Te_3 + 6Ln + 13Te$ resulting in a product ratio ALn_3Te_8:$A_2Te_3 = 1{:}1$ was used for the synthesis of the 1:3:8 compounds. The ampoules were heated according to the following temperature program: increase within 20 h to 650°C, annealing at this temperature for 12 h, cooling down within 125 h to 480°C, cooling down within 14 d to 280°C and finally annealing at 280°C for another 14 d. After this period the ampoules were quenched in ice water.

2.2. Physical properties measurements

Magnetic data were recorded with samples synthesized by the flux technique after extraction with DMF and enclosed in gelatin capsules, which were again sealed in Suprasil glass capillaries of 200 mm length and a reduction in the middle of the capillaries to hold the gelatin capsule. Susceptibility measurements were performed with an MPMS SQUID magnetometer (Quantum Design) as a function of magnetic field strength from 320 K down to 5 K. Because of the paramagnetic

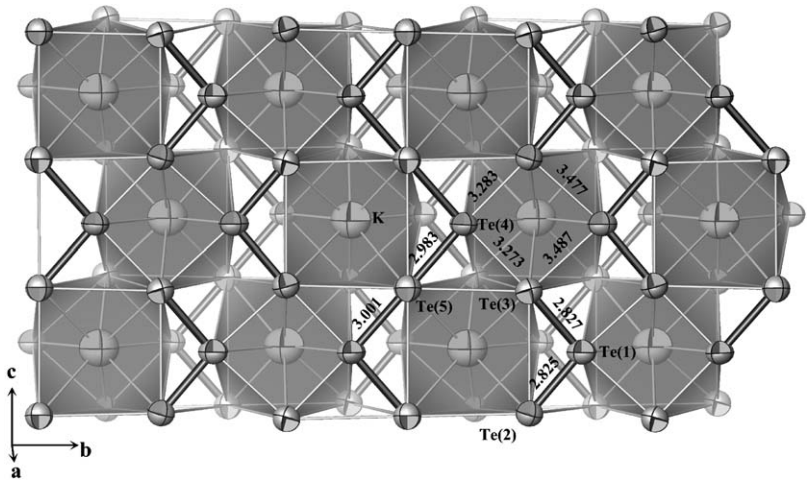

Fig. 3. Details of the ALn_3Q_8 crystal structure (A= K and Ln=Pr, Nd) in a projection along [100] emphasizing the coordination polyhedra of the alkali metal ions (gray). Four layers of ions in the sequence Te–K–K–Te with Te in the form of distorted and depleted 4^4 nets are shown. Interatomic distances in Å.

nature of the compounds no diamagnetic corrections were applied.

Resistance measurements were performed by a standard four-probe technique according to van der Pauw [16]. As samples die-shaped single-crystals or pressed pellets of powdered samples were used, and the resistance was measured within the temperature interval of $T = 5-300$ K.

3. Details of the electronic band structure calculations

3.1. LDA LMTO-ASA calculations

The self-consistent ab initio band structure calculations have been performed using density functional theory in the local density approximation (LDA) with the LMTO-47 package of Andersen et al. [17]. For the calculations the structural parameters of $KPrTe_4$, $KNdTe_4$, $RbNdTe_4$, $CsNdTe_4$, KPr_3Te_8 and KNd_3Te_8 already published in Refs. [4–6,9] served as the bases. The parameters of those compounds, whose band structures are explicitly treated in the following sections, are summarized in Table 1. The calculation within the atomic spheres approximation (ASA) includes corrections for the neglect of the interstitial region and the partial waves of higher order (ASA + combined correction). To reduce the overlap between the atomic spheres as much as possible, empty interstitial spheres were added to the potential. The construction of the ASA radii was performed by an automatical procedure of the program package using the method proposed by Andersen [18]. In detail the sphere radii are given in Table 2 for those compounds explicitly treated in this manuscript. For the other compounds the corresponding values were determined in a similar way. The basis set consisted of the K, Rb, Cs *ns* LMTOs, the Pr, Nd and Gd 6*s*, 5*d* and 4*f* LMTOs,[1] the Te 5*s* and 5*p* LMTOs, and the interstitial 1*s* and 2*p* LMTOs. The K, Rb, Cs *np*, $(n-1)d$ and $(n-1)f$, the Pr, Nd and Gd 6*p*, the Te 5*d* and 4*f*, and the interstitial *d* partial waves were included only in the tails of these LMTOs according to the Löwdin down-folding procedure [18]. The $\vec{k}$-space integration was performed by the tetrahedron method. Charge self-consistency and properties calculations were

Table 1
Structure data of all compounds, whose band structure is explicitly treated in the text

$ALnTe_4$, space group $P4/nbm$, A (2*a*) $\frac{1}{4}\frac{1}{4}0$, Ln (2*b*) $\frac{1}{4}\frac{1}{4}\frac{1}{2}$, and Te (8*m*) $x\,\bar{x}\,z$

Compound	a (Å)	c (Å)	x/a	z/c
$KNdTe_4$	6.9109	8.7407	0.10778	0.28475
$KGdTe_4$	6.843	8.6756	0.1065	0.28849

KPr_3Te_8, space group $P2_1/c$, K, Pr and Te (4*e*) *xyz*

a (Å)	b (Å)	c (Å)	β (°)
13.9058	12.9106	9.0018	99.264

Atom	x/a	y/b	z/c
K	0.0354	0.4080	0.2583
Pr(1)	0.34957	0.41513	0.08103
Pr(2)	0.35124	0.08397	0.09466
Pr(3)	0.65506	0.25066	0.41329
Te(1)	0.15818	0.72148	0.28997
Te(2)	0.16536	0.58002	0.05254
Te(3)	0.16590	0.57933	0.53053
Te(4)	0.16882	0.09733	0.29202
Te(5)	0.16951	0.24930	0.04263
Te(6)	0.41632	0.25471	0.35430
Te(7)	0.58792	0.41435	0.14460
Te(8)	0.58913	0.07980	0.14921

[1] All attempts to include the Ln 4*f* states into the core and treat them as localized orbitals resulted in unbound core states.

Table 2
Muffin tin sphere radii (in Å) used in the spin-polarized LMTO-ASA calculations

Compound	*A*	*Ln*	Te	*E*	*E*(1)	*E*(2)
$KNdTe_4$	(2*a*) 2.572	(2*b*) 2.133	(8*m*) 1.587	(2*c*) 1.372	(2*d*) 1.083	(8*m*) 0.934
$KGdTe_4$	(2*a*) 2.561	(2*b*) 2.077	(8*m*) 1.586	(2*c*) 1.348	(2*d*) 1.042	(8*m*) 0.928

Compound	K	Pr(1)	Pr(2)	Pr(3)	Te(1)	Te(2)
KPr_3Te_8	(4*e*) 2.388	(4*e*) 1.930	(4*e*) 1.944	(4*e*) 1.944	(4*e*) 1.638	(4*e*) 1.639
	Te(3)	Te(4)	Te(5)	Te(6)	Te(7)	Te(8)
	(4*e*) 1.642	(4*e*) 1.728	(4*e*) 1.732	(4*e*) 1.808	(4*e*) 1.792	(4*e*) 1.825
	E	*E*(1)	*E*(2)	*E*(3)	*E*(4)	*E*(5)
	(4*e*) 1.501	(4*e*) 1.508	(4*e*) 1.286	(4*e*) 1.247	(4*e*) 1.208	(4*e*) 1.155
	E(6)	*E*(7)	*E*(8)			
	(4*e*) 1.126	(4*e*) 1.136	(4*e*) 1.096			

obtained from 225 ($KPrTe_4$, $KNdTe_4$, $RbNdTe_4$, $CsNdTe_4$ and $KGdTe_4$) and 80 irreducible $\vec{k}$-points (KPr_3Te_8 and KNd_3Te_8). As a measure for the bonding strengths we computed the crystal orbital Hamiltonian population (COHP) function which is the Hamiltonian population weighted density of states. As recommended [19], a reduced basis set, in which all empty sphere LMTOs have been down-folded, was used for the COHP calculation. For the discussion of the bonding characteristics the well implemented electron localization function (ELF) [20] was calculated. In the implementation for density functional theory [21] this quantity depends on the excess of local kinetic energy due to the Pauli principle compared with the non-interacting bosonic system. Regions in space, where the Pauli principle does not lead to a rise of the kinetic energy density of the electrons (high value of ELF), can be identified as regions, where pairing of electrons with different spin plays an important role. High values of ELF can therefore be found in regions of high electron localization like covalent bonds or lone pairs.

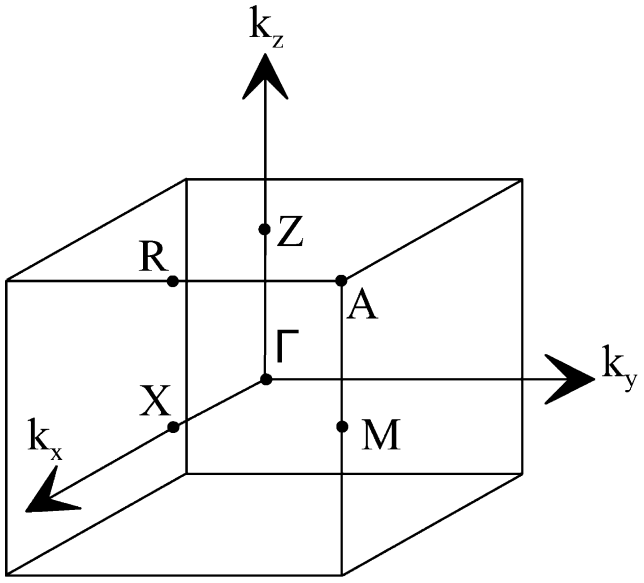

Fig. 4. Brillouin zones of $ALnTe_4$ compounds with high symmetry points.

3.2. Brillouin zone

The reciprocal lattice vectors of the $ALnTe_4$ compounds together with the first Brillouin zone are shown in Fig. 4. High symmetry points were labeled following Miller and Love [22].

3.3. EH calculations

For the purpose of comparison with the LMTO results and for didactic reasons we also performed extended-Hückel calculations using the program EHMACC [23].

4. Results of the LMTO-ASA energy band calculations

In quantum mechanical band structure calculations the general problem appears that most programs underestimate the correlation energies of the 4*f* or 5*f* states in lanthanoids or actinides, respectively, so that in non-magnetic calculations always narrow *f*-bands are observed at the Fermi level, the only exception being programs using the LSDA + U formalism such as WIEN2k, which are numerically very expensive in the case of larger problems such as the ALn_3Te_8 compounds. To avoid this problem in LMTO calculations it was suggested to perform spin-polarized band structure calculations. It is known [24] that in spin-polarized calculations the 4*f* or 5*f* population difference Δ, defined as $n\uparrow - n\downarrow$, is maximal for complete localized systems and zero for itinerant systems. The stronger the overlap of the *f* wave functions, the larger is the width of the *f* bands and the smaller is the density of states at the Fermi level and the population difference Δ (Hubbard like model). The assumption of 4*f* polarization in the investigated compounds is founded by the observation of paramagnetic behavior with magnetic moments

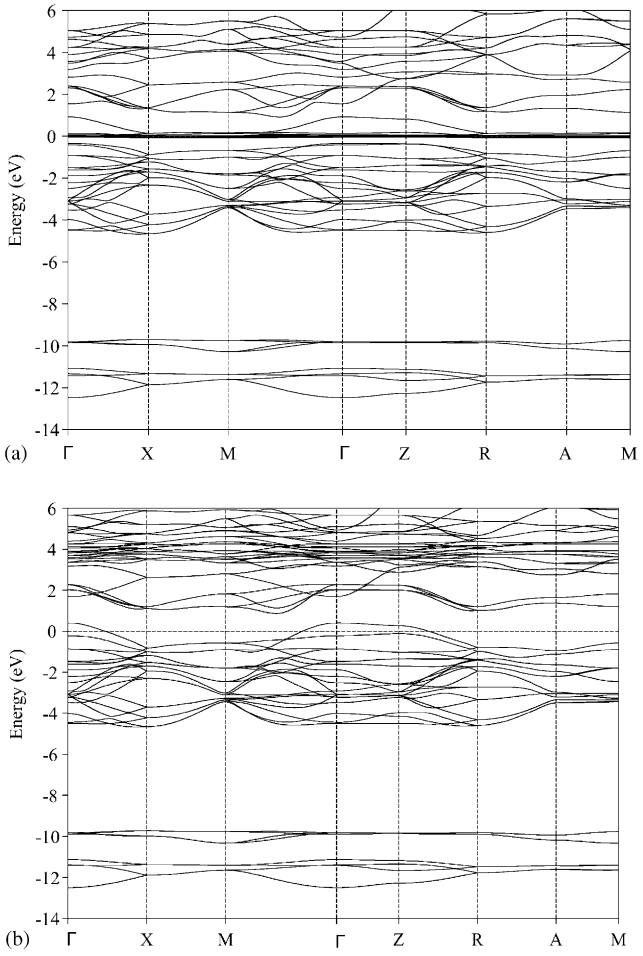

Fig. 5. Energy bands of $KNdTe_4$ (a) spin-majority and (b) spin-minority component.

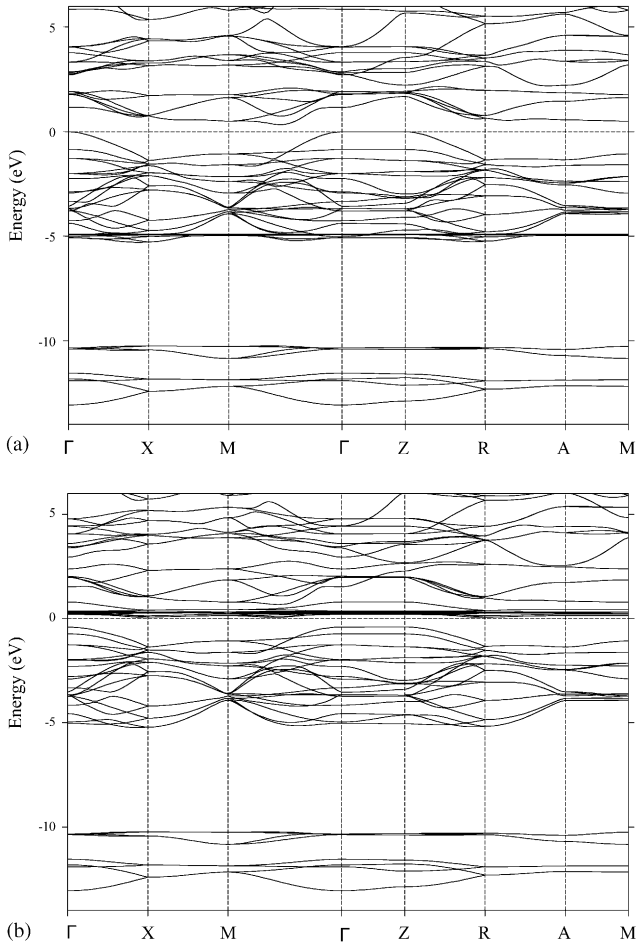

Fig. 6. Energy bands of $KGdTe_4$ (a) spin-majority and (b) spin-minority component.

comparable to those of the free ions in susceptibility measurements (see below). Additional to spin-polarized calculations, we performed non-magnetic calculations resulting in band structures always identical to those of the spin majority component in the spin-polarized calculations.

The calculated energy band structure of the $ALnTe_4$ compounds is shown exemplarily for the compounds $KNdTe_4$ and $KGdTe_4$ in Figs. 5 and 6, respectively, for the wave vector $\vec{k}$ along the following lines (see Fig. 4): $\Gamma = (0,0,0)$ to $X = (0,\frac{1}{2},0)$ to $M = (\frac{1}{2},\frac{1}{2},0)$ and then back to $\Gamma = (0,0,0)$, and further on to $Z = (0,0,\frac{1}{2})$ to $R = (0,\frac{1}{2},\frac{1}{2})$ to $A = (\frac{1}{2},\frac{1}{2},\frac{1}{2})$ and finally to $M = (\frac{1}{2},\frac{1}{2},0)$. In Figs. 5a and 6a the spin-majority bands and in Figs. 5b and 6b the spin-minority bands are shown. The coordinates are given in units of the reciprocal lattice vectors. The band structure was projected onto orthogonal LMTOs normalized to unity within the ASA spheres: the $5p_x$, $5p_y$ and $5p_z$ orbitals of Te, the ns orbitals of A, as well as the $4f$ and $5d$ orbitals of Ln. In such a 'fat' band structure—examples are given in Fig. 7a–d—each band is given a width which is proportional to the weight or the sum of the weights of the corresponding orbital or orbitals. In all the three figures an orbital character of 100% is equivalent to $\frac{1}{20}$ of the total energy scale. For a scale of -14 to 6 eV this is 1 eV. For the sake of representation, we set the Fermi energy $E_F = 0$ eV in these figures and throughout this paper.

In the primitive tetragonal unit cell there are two formula units $ALnTe_4$. The total number of four $[Te_2]^{2-}$ dumbbells is separated into two layers with two dumbbells each. From this a total number of 32 valence bands with mainly Te contributions is to be calculated. Contributions mainly of the Te $5s$ states are seen in the range -14 to -10 eV (eight bands), whereas bands above -5 eV to E_F are mainly Te $5p$-centered states. Additionally, Gd $4f$ states are found for the spin majority component at -5 eV in $KGdTe_4$ (Fig. 6a). For the other investigated $ALnTe_4$ compounds the $4f$ states appear directly at the Fermi level in the spin majority band structure and directly above ($KGdTe_4$) or well above in the spin-minority band structure. The latter is also true for the $5d$ Ln- and K, Rb, Cs

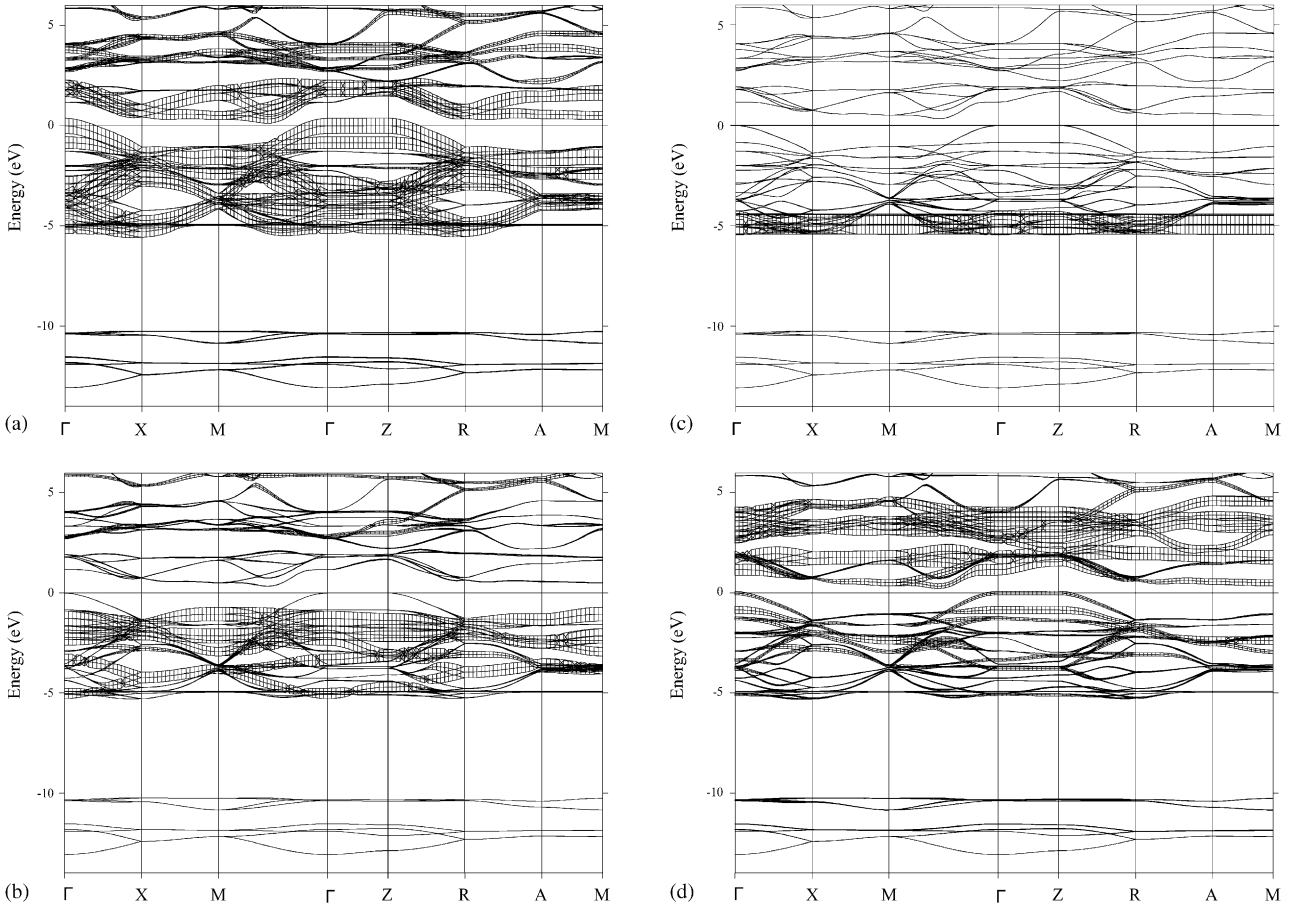

Fig. 7. Energy bands of the spin-majority component of $KGdTe_4$ decorated with orthonormal-orbital characters. A pure band state is given the energy width 1.0 eV. (a) Te $5p_{xy}$ 'fat' bands, (b) Te $5p_z$ 'fat' bands, (c) Gd $4f$ 'fat' bands and (d) Gd $5d$ 'fat' bands.

ns-centered states. With two dumbbells in each layer at the two different heights z and $\bar{z}$ there are also four Te–Te antibonding $pp\sigma^*$-bands above E_F (see Fig. 7a). To illustrate this we performed EH band structure calculations of an isolated $4.3^2.4.3$ net of tellurium with interatomic distances taken from $KNdTe_4$ (2.78 Å intradumbbell and 3.76 Å interdumbbell distance), which are depicted in Fig. 8. In the translational unit there are now only two dumbbells, whereas the complete polyanionic partial structure of the $ALnTe_4$ compounds is built up from two such nets rotated by 90°, so that in the [001] direction the dumbbells are staggered crosswise to rods (see Fig. 1). With only two dumbbells per unit cell, there are two $pp\sigma^*$ bands above E_F—the Fermi level corresponding to $[Te_2]^{2-}$ units. At the zone center Γ these two bands—numbered as 15 and 16—are degenerated and their completely antibonding character can readily be taken from the representation of the orbital characters at the zone center in Fig. 8. They correspond to band numbers 5 and 7, the Te–Te $pp\sigma$ bonding bands. All other bands can be grouped into $pp\pi$ bonding and $pp\pi^*$ antibonding, but since these are completely occupied, they have to be interpreted as lone pairs of classical $[Te_2]^{2-}$ units. At the zone boundaries X and M most of the bands degenerate, the most pronounced dispersion revealing bands 10 and 14. Because the σ bond within the dumbbells is an interaction within one unit cell, the corresponding bands show (almost) no dispersion. Bands 10 and 14 are $p_{xy}p_{xy}\pi^*$ antibonding within the dumbbells, the difference between the two being that they are $p_{xy}p_{xy}\pi$ bonding (no. 10) and $p_{xy}p_{xy}\pi^*$ antibonding (no. 14) with respect to the interdumbbell interaction. At point X they degenerate to bands 10′ and 14′.

A point, which was already discussed in detail in the structural part of this contribution, was the clear differentiation of the homonuclear distances into intra and interdumbbell interactions in this type of compound. The discussion of this in polytellurides rather untypical situation was performed only on the basis of geometrical arguments. But the question arises whether this situation is also reflected in the quantum chemical calculations. So we performed calculations of the ELF and COHP calculations.

The total ELF (compared to the valence ELF) is shown in Fig. 9 for $KNdTe_4$ in a two-dimensional

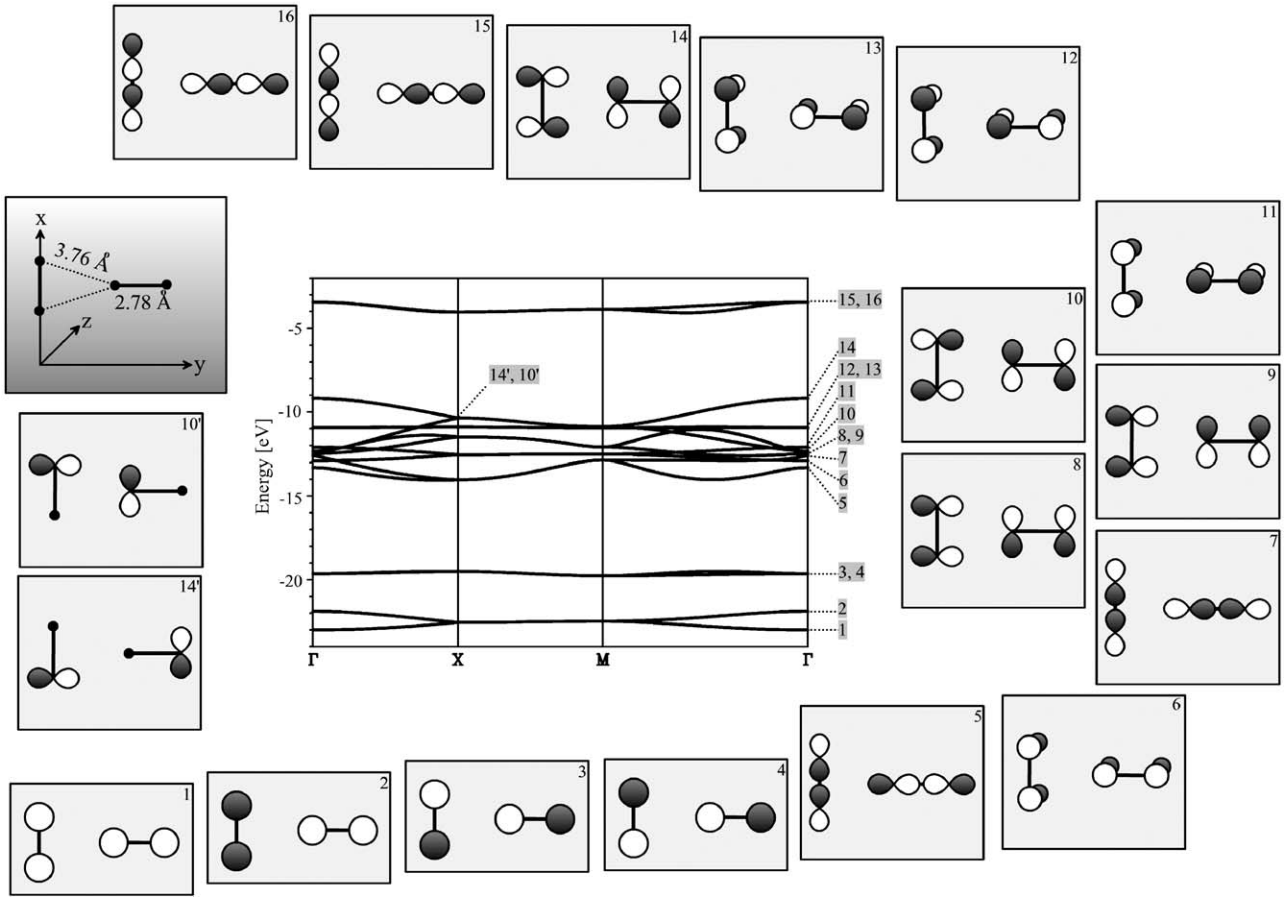

Fig. 8. EH band structure of an isolated $4.3^2.4.3$ Te net with dimensions taken from $KNdTe_4$ including a simplified crystal orbital analysis at the zone center Γ. As Hückel parameters for Te $H_{ii}(5s) = -20.8$ eV, $\xi(5s) = 2.51$ and $H_{ii}(5p) = -11.8$ eV, $\xi(5p) = 2.16$ were used.

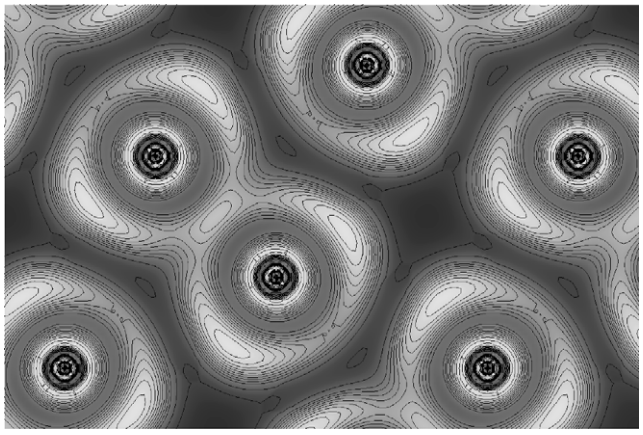

Fig. 9. Section of the total 3*d*-ELF through the polyanionic partial structure in $KNdTe_4$ parallel to the a_1a_2 plane with $[Te_2]$ dumbbells. Regions of high localization are bright, and those of low localization are dark. Clearly the covalent attractor in the center of each dumbbell can be seen.

section running through a polyanionic Te layer at height z. Clearly isolated $[Te_2]$ units are presented, which are separated by regions with ELF values lower than 0.2. Apart from lone pair attractors around Te a covalent attractor for each dumbbell can also be readily recognized from Fig. 9. Integration within the limits of the corresponding basin yields the basin population [25]. With the valence density a population of 0.68 electrons and with the total density a value of 0.81 electrons was calculated [26], both being much lower than assumed in the usual picture of a two-center two-electron bond. This behavior is typical for tellurides and we will comment on it in a separate contribution.

Another indication for the assumption of isolated $[Te_2]^{2-}$ units comes from the COHP calculations, which gives results similar to those of the well-known COOP. The results of our calculations are presented for the spin-majority and minority components of $KNdTe_4$ in Fig. 10, together with the corresponding integrated COHP curves. ICOHP values at the Fermi level are also given. We note that the two symmetry-independent Te–Te interactions—the intradumbbell interaction with 2.78 Å and the interdumbbell interaction with 3.76 Å—show the expected behavior: the energy sequence of the orbital interactions being $ss\sigma$, $ss\sigma^*$, $pp\sigma$, $pp\pi$, $pp\pi^*$ (all occupied) and $pp\sigma^*$ above E_F (unoccupied), for the short intradumbbell interaction an ICOHP value of 2.01 eV per cell and bond (↑plus↓) and for the long interdumb-

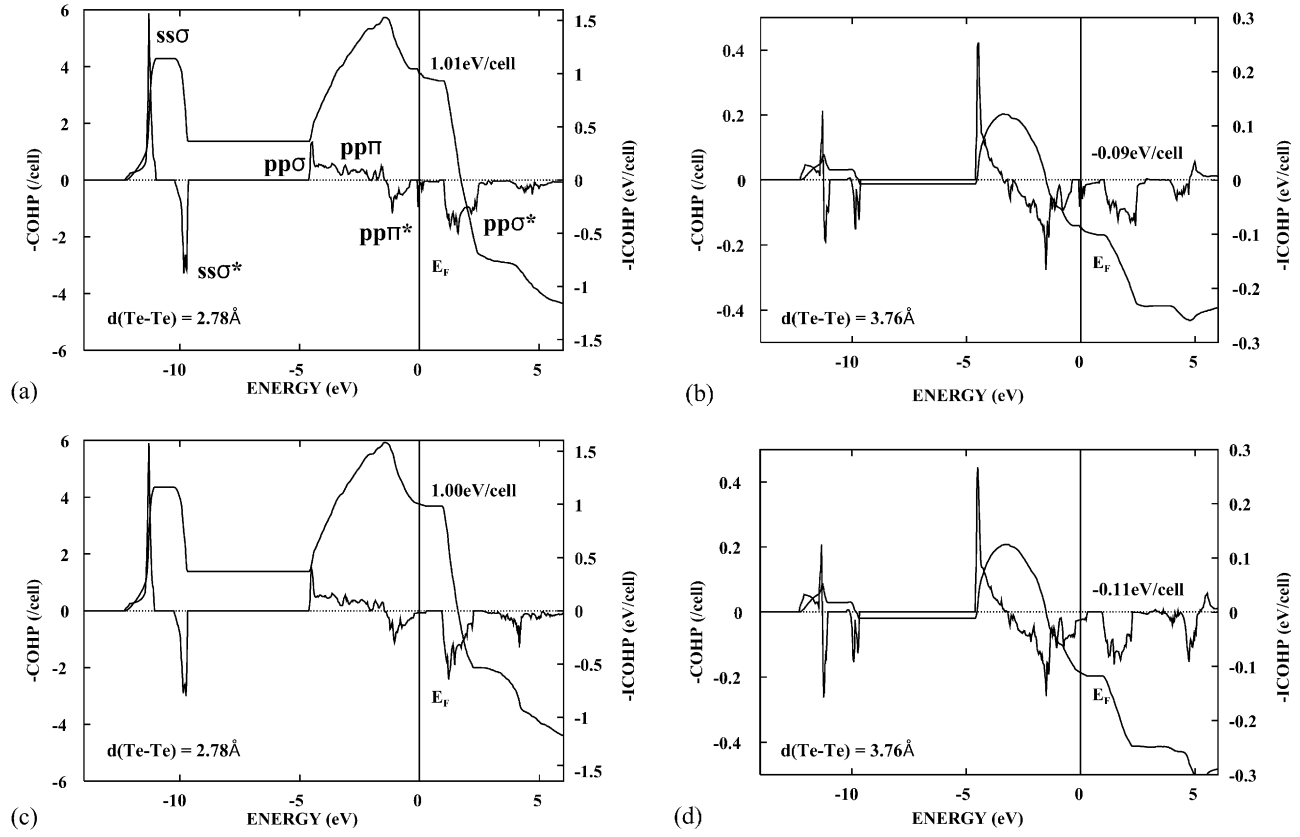

Fig. 10. COHP for $KNdTe_4$. (a) Spin-majority intradumbbell, (b) spin-majority interdumbbell, (c) spin-minority intradumbbell and (d) spin-minority interdumbbell interaction. The integrated COHP values up to the Fermi level are given per cell and bond.

bell interaction a value of ICOHP = −0.20 eV per cell was calculated. This clearly indicates that there is no bonding, even some antibonding interaction between the dumbbells.

Looking at the COHP curves in detail, especially around the Fermi level, we find that again the problem of the 4*f* states in LMTO calculations evolves. In the COHP of the spin-majority component at E_F three sharp spikes can be seen in Fig. 10a and b, which originate from an admixture of Te *p* states with the 4*f* levels of Nd, and additionally a small pseudo-band gap below E_F of about 0.2 eV. The corresponding band structure was shown in Fig. 5a. On the other hand these structures are missing in the COHP and band structure of the spin-minority component (Fig. 10c and d). Nevertheless both indicate that $KNdTe_4$ should be a metallic conductor. This result is insofar surprising that considering the dumbbells as purely $[Te_2]^{2-}$ units as in the EH calculations of Fig. 8 and in the formulation of these compounds as $\{A^+Ln^{3+}([Te_2]^{2-})_2\}$, at first glance we expect semiconducting behavior. To investigate this finding in more detail, we also performed band structure calculations on the Rb and Cs homologues of $KNdTe_4$ and we also varied the rare earth cations for the same *A* cation. For this purpose structural data were available for $KPrTe_4$ and $KGdTe_4$.

By varying the cations two trends can be observed: changing the alkali metal from K to Rb and Cs has almost no influence on the band structure. $RbNdTe_4$ and $CsNdTe_4$ should also be metallic. On the other hand changing the rare earth ions has a significant influence on the band structure. Whereas the main features of the band structures of these isotypic compounds are not involved, characteristic variations in the difference between the maximum of the $p_{xy}p_{xy}\pi^*$ bands energy above E_F—being maximal at the zone center Γ—and the Fermi level are to be recognized. The course of this difference is the same for the spin-majority and the spin-minority components: we found that $\Delta E(\mathrm{Pr}) \lesssim \Delta E(\mathrm{Nd}) > \Delta E(\mathrm{Gd})$, the latter being zero or even negative for the spin-majority and minority components, respectively. From this we have to conclude that in contrast to $KPrTe_4$ and $KNdTe_4$ the compound $KGdTe_4$ should be semiconducting. In principle we have to consider a number of effects influencing the position of the center and width of the Te *pp* bands. First of all we have to mention here the interatomic distances within the Te nets: especially the interdumbbell distance is directly reflecting the dispersion of the *pp* bands. At the bottom and the top of the *pp* bands moiety we found the $pp\sigma$ bonding and $pp\pi^*$ antibonding interactions (see Fig. 8: bands 5 and 14), so

that on a decrease of the interdumbbell distance (from $KNdTe_4$ to $KGdTe_4$) the width of the Te *pp* bands increases. On the other hand the admixture of 4*f* and 5*d* states of the rare earth cations is influencing the energy of the Te *pp* bands. E.g., in Fig. 6b we can see that along the line Γ to Z the band at the top of the Te *pp* bands is lowered due to 4*f* mixing in favor of a single state mainly of 4*f* character, which is increased in energy. All in all, the complete Te *pp* band entity is lowered in energy in $KGdTe_4$ at about 0.5 eV. Due to the increased stability of a half-filled 4*f* shell each Te has a formal higher charge in this compound, i.e. there is a higher electron carryover from the rare earth metal ions onto the anions in $KGdTe_4$ than in the other two potassium compounds. From this, the formulation of $KGdTe_4$ as $\{K^+\ Gd^{3+}\ ([Te_2]^{2-})_2\}$ is adequate, but not in an analogous way for the other compounds. Due to a high degree of covalency—meaning an incomplete carryover of valence electrons from *Ln* to Te—in all other *ALn*Te4 compounds investigated so far, the $pp\pi^*$ bands are not completely filled resulting in metallic behavior. The results of resistivity measurements together with magnetic susceptibility measurements are given exemplarily for $KNdTe_4$ in Fig. 11a and b, respectively. From the linear relationship of the inverse susceptibility data $1/\chi_{mol}$ versus T above $T = 25$ K a magnetic moment of $\mu = 3.54$ BM was calculated compared to a magnetic moment of $\mu = 3.62$ BM of the free Nd^{3+} ion with a ground-state term of $^4I_{9/2}$ for the electron configuration $4f^3$. Down to $T = 2$ K no indications for a magnetic ordering can be seen, the paramagnetic Curie temperature being $\Theta_p = -9.6$ K, independent of the applied magnetic field. This is consistent with the results of the spin-polarized band structure calculations giving for Nd in $KNdTe_4$ a $\Delta = n\uparrow - n\downarrow \approx 3$ electrons. The temperature behavior of the mean resistivity above $T = 200$ K clearly indicated metallic conductivity. At $T = 195(5)$K a minimum in resistivity is observed followed by an increase of resistivity at lower temperatures of almost one order of magnitude. We attribute this minimum to a metal–insulator transition, the nature of this transition being at the moment completely unknown. All in all, we have to conclude that the results of the band structure calculations for the $ALnTe_4$ compounds known so far are in excellent agreement with the results of the physical properties measurements.

Representatives of the second family of compounds are the compounds KPr_3Te_8 and KNd_3Te_8, which crystallized as addition-defect variants of the $NdTe_3$ structure type as mentioned above. The eight crystallographically different Te atomic positions of Wyckoff notation (4*e*) can be divided into two groups: Te(5–8) forming one group are simply Te^{2-} ions in the distorted rock-salt type building blocks. Te(1–3) are forming the L-shaped $[Te_3]^{2-}$ units and Te(4–5) the infinite zig-zag chains $^1_\infty[Te_4]^{4-}$ running in the [001] direction. Te(1–5) are forming the second group and are arranged as depleted and distorted 4^4 nets parallel to the *bc*-plane of

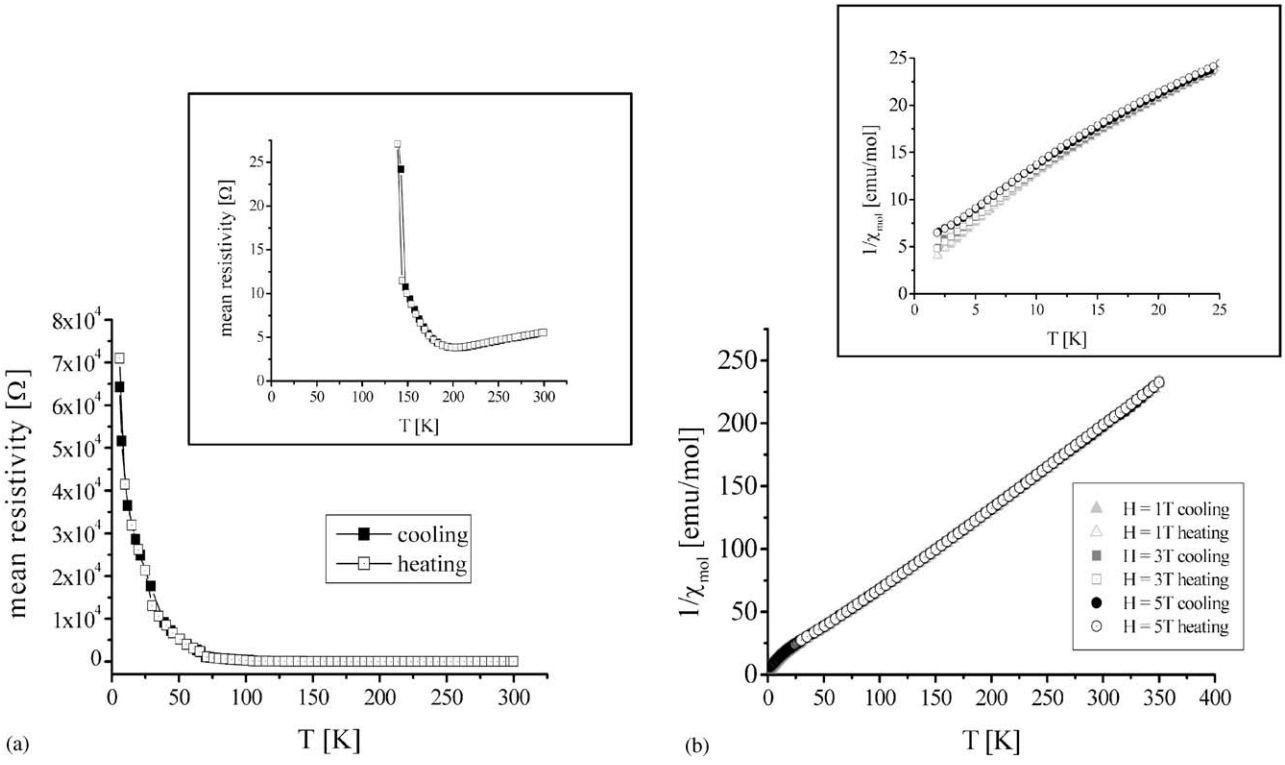

Fig. 11. (a) Resistivity (inset: low resistivity region) and (b) magnetic susceptibility data of $KNdTe_4$ (inset: low temperature details).

the unit cell. Let us discuss these two building blocks one after the other.

As we have already seen in the crystal structure section, the geometry of the L-shaped $[Te_3]^{2-}$ units in the ALn_3Te_8 compounds is comparable to those in the alkali metal sesquitellurides, the only difference being secondary interatomic distances to the neighboring zig-zag chains in the range of 3.27–3.28 Å and from triatomic unit to the other in the range of 3.48–3.49 Å. Following this argumentation we regard the $[Te_3]^{2-}$ as classical 20 electron species. For this species we indeed expect an L-shaped geometry, whereas for 22 electrons we observe a linear arrangement. A Walsh diagram for the two geometries of a triatomic species is given in Fig. 12. The linear triatomic $[Te_3]^{4-}$ unit is isolectronic to the well known $[I_3]^-$ ion or the neutral XeF_2 molecule. On the other hand, as 21 electron species the unit $[Te_3]^{3-}$ was observed in TlTe, where it dimerizes forming at temperatures below $T = 172$ K a new type of 42 electron $[Te_6]^{6-}$ partial structure formerly not known in polyhalide or noble gas halogenide chemistry [27]. To answer the question of possible interactions between polyanionic units observed in this type of compound we again calculated the COHP function, whereas the calculated energy band structures of the ALn_3Te_8 compounds are not shown, since these are very complex with 48 atoms per unit cell (four formula units). Examples for calculated COHP curves are given in Fig. 13a–d. In almost the same manner as electronic band structures they reveal that there is a band gap at the Fermi level indicating the semiconducting behavior of the ALn_3Te_8 compounds. The results of the COHP calculations are also summarized in Table 3, which gives the sum of the ICOHP values of both, the spin-majority and minority components, for all relevant Te–Te interactions. The reason for this is the fact that the values for spin up and down differ only marginally due to the influence by the spin polarization caused by *Ln*. From Table 3 the homonuclear interactions can be subdivided into three groups: the maxima are found for the interactions within the $[Te_3]^{2-}$ units with ICOHP values of 1.83 and 1.85 eV per bond and cell. Again *ss* and *pp* bonding and antibonding interactions can clearly be differentiated. As typical generally for Te ions with partial negative charges up to the Fermi level already $pp\pi^*$ antibonding states are occupied reducing the bond order in most cases into the range of partial bonds. The second group of interactions is formed by the bonds

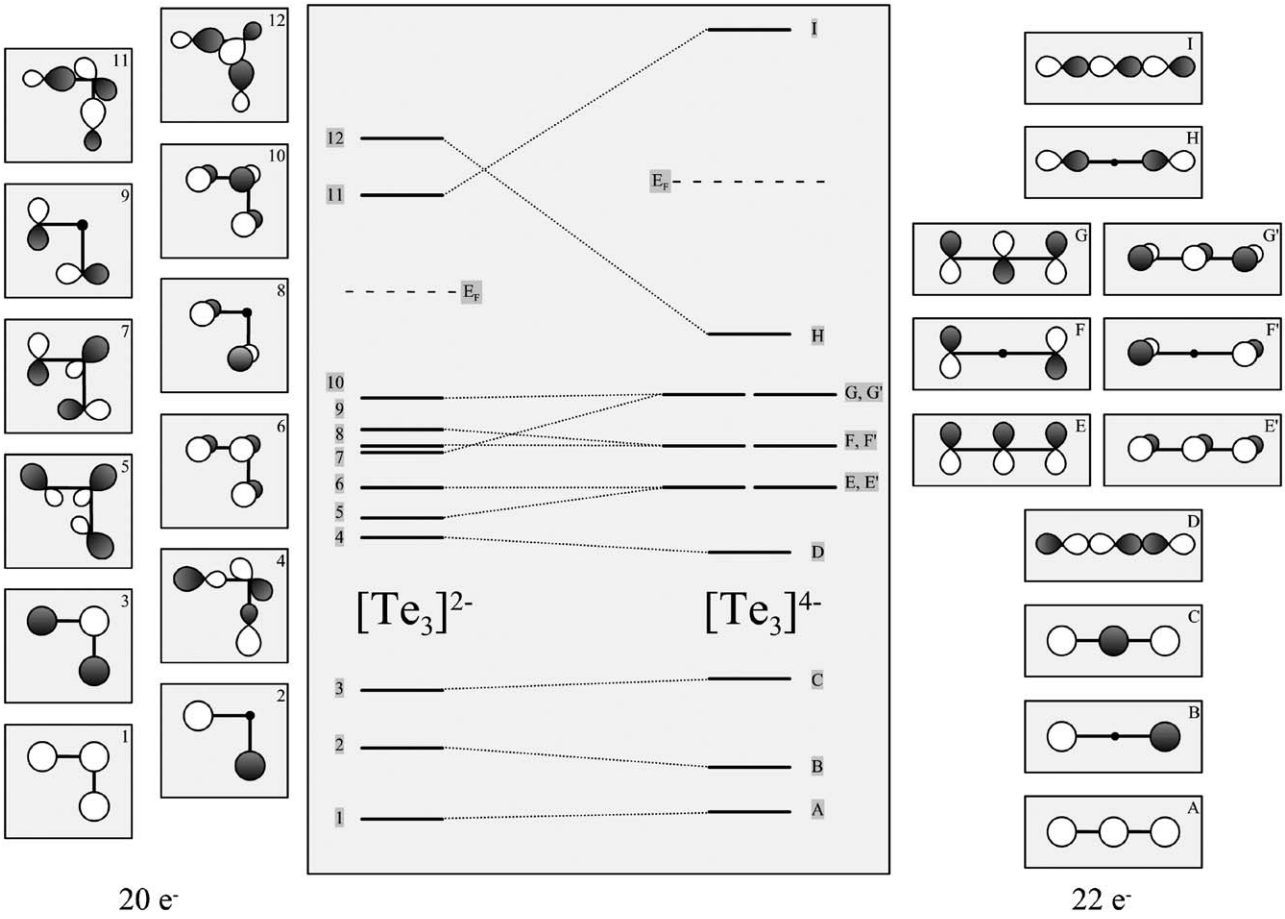

Fig. 12. Walsh diagram for triatomic $[Te_3]$ units. Left: L-shaped 20 electron, right side: linear 22 electron species.

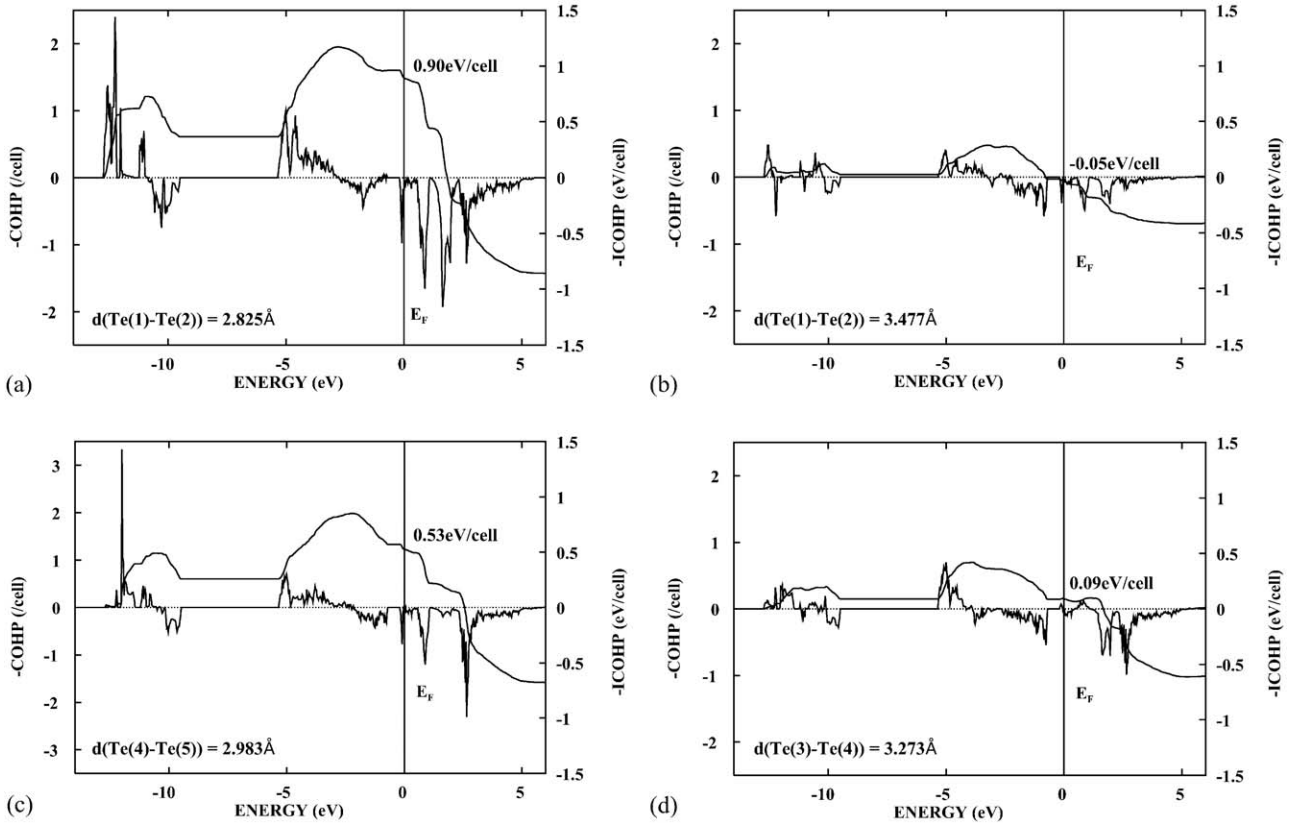

Fig. 13. COHP for the spin-majority component of KPr_3Te_8. (a) Te(1)–Te(2) with 2.825 Å, (b) Te(1)–Te(2) with 3.477 Å, (c) Te(4)–Te(5) with 2.983 Å and (d) Te(3)–Te(4) with 3.273 Å.The integrated COHP values up to the Fermi level are given per cell and bond.

Table 3
Results of the COHP calculations for KPr_3Te_8. ICOHP values are given in eV per cell and bond

Atoms	Distance (Å)	ICOHP = ICOHP↑ + ICOHP↓
Te(1)–Te(2)	2.825	1.85
Te(1)–Te(3)	2.827	1.83
Te(1)–Te(2)	3.477	−0.08
Te(1)–Te(3)	3.487	−0.09
Te(4)–Te(5)	2.983	1.09
Te(4)–Te(5)	3.001	1.01
Te(2)–Te(4)	3.283	0.14
Te(3)–Te(4)	3.273	0.16

within the infinite zig-zag chains with ICOHP values of 1.01 and 1.09 eV per cell and bond. The individual values within this compound allow us to gauge the strengths of the interactions one below the other. Relative to the interactions within the $[Te_3]^{2-}$ units we have to recognize that the bonds within the infinite chains are considerably weaker. For all other interactions the ICOHP values are lower than 0.16 eV per cell and bond or even are completely non-bonding. Correspondingly, the calculations made it evident that among the different homonuclear interactions only those with $d < 3.20$ Å are of considerable interest. This supports our view of the ALn_3Q_8 compounds of the KNd_3Te_8 structure type as being built from isolated L-shaped $[Te_3]^{2-}$ and infinite zig-zag chains $^1_\infty[Te_4]^{4-}$.

Finally, we will look at the infinite zig-zag chain $^1_\infty[Te_4]^{4-}$ in more detail. Formally the zig-zag chains can be considered as built exactly from the two triatomic species already discussed above, i.e. the L-shaped 20 electron species $[Te_3]^{2-}$ and the linear 22 electron species $[Te_3]^{4-}$ (see Fig. 12). This is depicted in Fig. 14a, together with two additional possibilities of generating this zig-zag chain from oligoatomic units (Fig. 14b and c) one can think of. Also in a purely formal way we can attribute each Te in this homonuclear chain a charge of −1. On the other hand chemists usually associate certain binding situations with definite electron counts. For example, a Te ion at the corner of a zig-zag chain (Te(4)) can be compared in terms of its CN to one in elemental tellurium, which is neutral, whereas the enlarged interatomic distances within the zig-zag chain compared to Te clearly indicate a higher charge. On the other hand comparing the linear 22 electron $[Te_3]^{4-}$ with the isoelectronic XeF_2 molecule would lead us formally to linear coordinated hypervalent Te^{2-} in the chain (Te(5)) again resulting in a charge of −4 for the complete zig-zag chain. But the question arises as to which one of these descriptions is adequate.

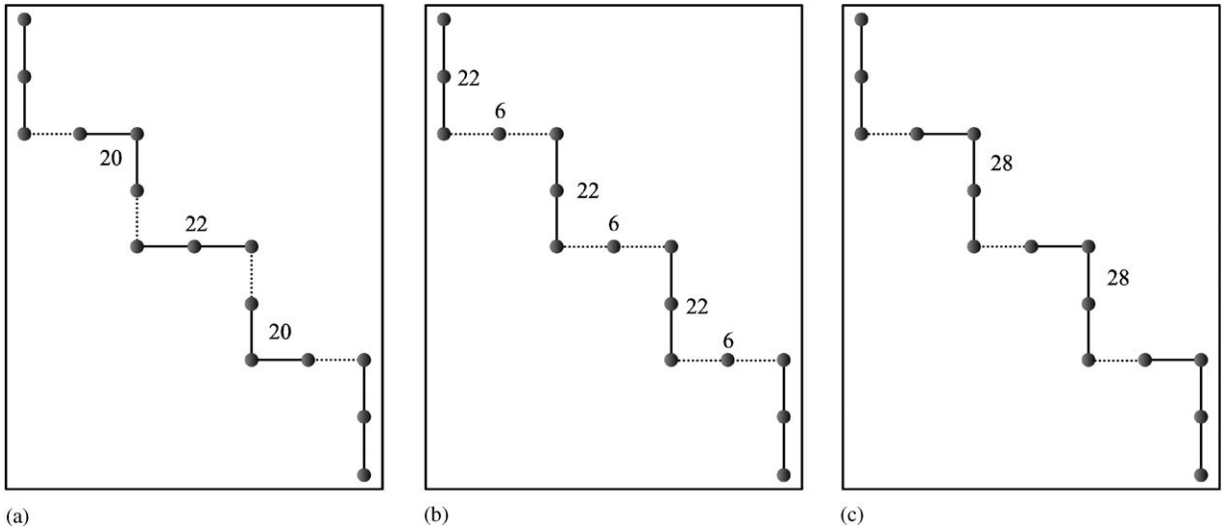

Fig. 14. Three possibilities of generating an infinite zig-zag chain $^{1}_{\infty}[Te_4]^{4-}$ from oligoatomic fragments with different electron counts.

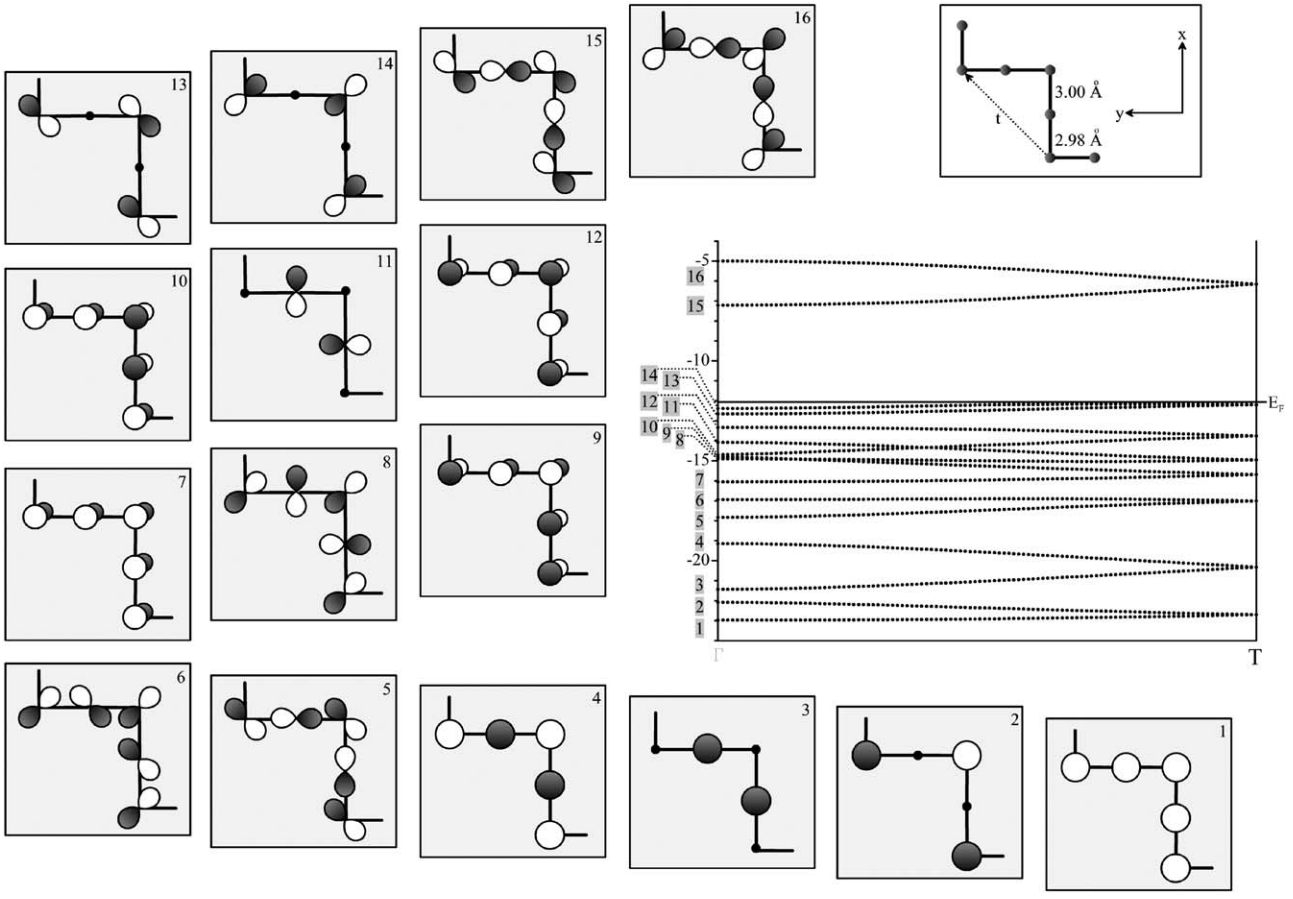

Fig. 15. EH band structure of an isolated infinite zig-zag chain $^{1}_{\infty}[Te_4]^{4-}$ with dimensions taken from KPr_3Te_8 including a simplified crystal orbital analysis at the zone center Γ. As Hückel parameters for Te $H_{ii}(5s) = -20.8$ eV, $\xi(5s) = 2.51$ and $H_{ii}(5p) = -11.8$ eV, $\xi(5p) = 2.16$ were used.

To answer this question we again performed EH calculations for the isolated zig-zag chain. An simplified orbital analysis at the zone center Γ is shown in Fig. 15. For the zig-zag chain we have four Te in the translational unit resulting in 16 bands filled with 28 electrons. Considering the two HOCOs 13 and 14 we

find that the largest p orbital coefficients are at the Te(4) ions, whereas they are almost zero at Te(5). Since this situation is true for the whole dispersion from Γ to T we have to conclude that in contrast to the descriptions above the most negative Te ion is Te(4) and not Te(5). The charge difference between the two ions is in a simple Mulliken population analysis of 0.17 electrons. But addition of K^+ ions to the zig-zag chains results in an increase of this difference to 0.27 electrons. The reason for this increase is the different K^+ coordination environment of Te(4) and Te(5). Each K^+ is surrounded by eight Te in the form of a distorted square anti-prism (see Fig. 3). Among the neighbors the two shortest K–Te distances are to Te(5) at distances 3.551 and 3.552 Å and the longest within this spectrum is to a single Te(4) with 3.719 Å. So K^+ is sucking off more electron density from Te(5) compared to Te(4) resulting in an increased charge difference of the two Te ions. Against chemists intuition the Te ions at the corners of the infinite zig-zag chain wear a higher negative charge than those in the middle.

Again we wanted to support the findings of the band structure calculations by experimental results. The corresponding resistivity data are depicted in Fig. 16 for KNd_3Te_8. At room temperature KNd_3Te_8 is an insulator and reveals at $T = 273(5)$K a reversible phase transition with a resistivity change of five orders of magnitude. For the phase at temperatures below the insulator to insulator transition a band gap energy of $E_0 = 153$ meV was extracted from a representation of $\ln(R/R_{290}) \cdot 2\,\mathrm{kT}$ versus T. As depicted in Fig. 16b the band gap is temperature dependent. From a fit of the linear part in Fig. 16b (black squares) the band gap can be extracted from the intersection point and the coefficient A ($E_g = E_0 - AT$) from the slope of the straight line. Again the nature of this low-temperature phase is completely unknown.

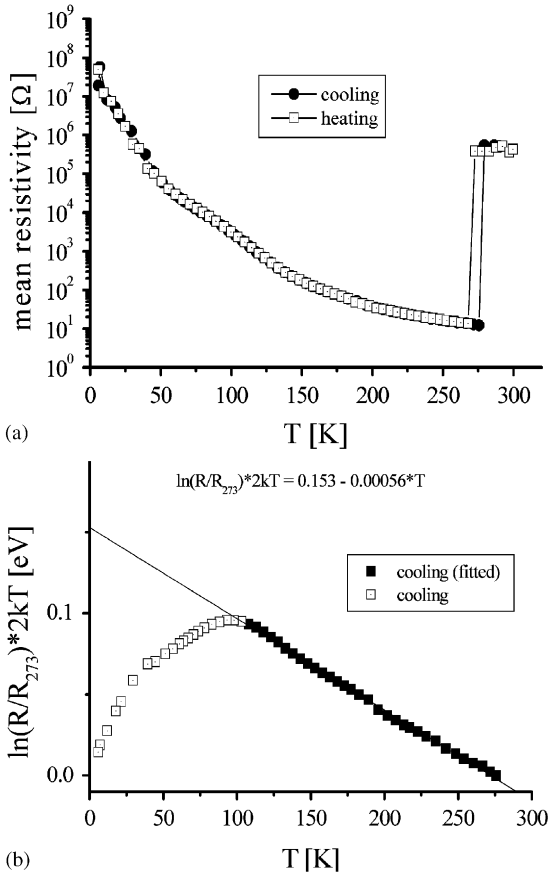

Fig. 16. Resistivity data of KNd_3Te_8, (a) R versus T and (b) $\ln(R/R_{290}) \cdot 2\,\mathrm{kT}$ versus T to estimate the band gap parameters E_0 and A in $E_g = E_0 - AT$.

5. Discussion

Our investigation of the band structures of a number of $ALnTe_4$ and ALn_3Te_8 compounds has shown that we sometimes obtain unforeseen results, if we rely only upon common concepts. In view of the structural polyanionic unit in the $ALnQ_4$ compounds, isolated $[Q_2]^{2-}$ dumbbells with typical single bond intradumbbell and non-bonding interdumbbell distances, and keeping in mind that isotypic selenides are also known [7], we would expect semiconducting behavior for these compounds. But as shown above, we have to differentiate our picture. For almost all investigated compounds, $KPrTe_4$, $KNdTe_4$, $RbNdTe_4$ and $CsNdTe_4$ band structure calculations indicate metallic behavior, only for $KGdTe_4$ semiconducting properties are to be deduced. For $KNdTe_4$ this predicted behavior was also verified experimentally. Also remarkable in this type of compounds is the topology of the polyanionic partial structure in the form of $4.3^2.4.3$ nets, which is not observed for any other polytelluride. Much more common are depleted and distorted 4^4 nets as, e.g., in $La_{10}Se_{19}$ [28] or $LaTe_2$ [2]. Lee and Foran [29] suggested that 90° HOMO-LUMO interactions between the dumbbells are responsible for the formation of certain arrangements in rare earth selenide superstructures. Especially in polytellurides, in many cases secondary interactions between the dumbbells are observed as in $LaTe_2$ with L-shaped dumbbell pairs. In the $ALnTe_4$ compounds investigated here, calculations of the ELF and COHP function revealed absolutely no significant interaction between the dumbbells.

This is not the case for the ALn_3Te_8 compounds, where there is still some, but not significant interaction between the structural units, L-shaped triatomic $[Te_3]^{2-}$ and infinite zig-zag chains $^1_\infty[Te_4]^{4-}$. The interatomic distances between these units (>3.27 Å) are too long for relevant secondary interactions. From the band structure calculation we were now able to give a more detailed picture of the charge distributions in these units.

From the HMO theory we would deduce the end-on Te in the 20 electron species $[Te_3]^{2-}$ having a charge of -1 and the central Te being neutral. The Walsh diagram for these triatomic units tells us that with 21 as well as 22 electrons a linear arrangement is favored. On the other hand, to give integral charges for the second unit, the zig-zag chains, it is not possible since the differences between the two types of Te ions are pronounced, but far from being integral. In contrast to well-accepted concepts we found the Te at the corners of the zig-zag chains being higher negatively charged than those in the middle of the tetra-atomic chain. Since the KLn_3Te_8 compounds (Ln = Pr, Nd) should be semiconducting—at the moment only verified for KNd_3Te_8—the situation is not predestined for the formation of charge density waves as observed for metallic systems as for example TlTe [27]. According to electron diffraction studies [9] indications for an additional, possibly incommensurate, superstructure along the chain axis are given suggesting an additional charge density wave. Our own single-crystal X-ray diffraction experiments on isotypic compounds of this type have revealed a very marked tendency of these compounds to form twins and polytypes with extended translation periods, which can also be another explanation for the observation of additional reflections in diffraction experiments. At the moment we have started to extend our investigations in two directions: first, to investigate the low-temperature polymorphs of the compounds mentioned above to solve their structures, and second, to try to optimize the geometry of the compounds investigated here by DFT PP methods.

Acknowledgments

We are gratefully indebted to Dr. R. K. Kremer, Mrs. E. Brücher and Mrs. G. Siegle, MPI for Solid State Research in Stuttgart, Germany, for the magnetic susceptibility and resististivity measurements. We also acknowledge the Deutschen Forschungsgemeinschaft and the Fonds der Chemischen Industrie for financial support.

References

[1] H. Schäfer, Contribution to a Discussion, Münster, Germany, 1962.
[2] K. Stöwe, J. Solid State Chem. 149 (2000) 155.
[3] H.G. Von Schnering, Angew. Chem. 93 (1981) 44.
[4] K. Stöwe, Ch. Napoli, S. Appel, Z. Anorg, Allg. Chem. 629 (2003) 321.
[5] K. Stöwe, Solid State Sci. 5 (2003) 765.
[6] K. Stöwe, Z. Anorg. Allg. Chem. 629 (2003) 403.
[7] A.C. Sutorik, M.G. Kanatzidis, Angew. Chem. 104 (1992) 1674.
[8] G. Llabres, O. Dideberg, L. Dupont, Acta Crystallogr. B28 (1972) 2438.
[9] R. Patschke, J. Heising, J.L. Schindler, C.R. Kannewurf, M. Kanatzidis, J. Solid State Chem. 135 (1998) 111.
[10] K. Norling, H. Steinfink, Inorg. Chem. 5 (1966) 1488.
[11] H. Bärnighausen, MATCH Comm. Math. Chem. 9 (1980) 139.
[12] C. Adenis, V. Langer, O. Lindqvist, Acta Crystallogr. C 45 (1989) 941.
[13] B. Eisenmann, H. Schäfer, Angew. Chem. 90 (1978) 731.
[14] K. Stöwe, Z. Kristallogr. 216 (2001) 215.
[15] M.G. Kanatzidis, A.C. Sutorik, Progr. Inorg. Chem. 43 (1995) 151.
[16] L.J. Van der Pauw, Philips Res. Rep. 13 (1958) 1.
[17] G. Krier, O. Jepsen, A. Burkhardt, O.K. Andersen, Tight binding LMTO-ASA Program Versions 4.7 and 4.7C, Stuttgart, Germany.
[18] O. Jepsen, O.K. Andersen, Z. Physik B 97 (1995) 35.
[19] F. Boucher, R. Rousseau, Inorg. Chem. 37 (1998) 2351.
[20] A.D. Becke, K.E. Edgecombe, J. Chem. Phys. 92 (1990) 5397.
[21] A. Savin, O. Jepsen, J. Flad, O.K. Andersen, H. Preuß, H.G. von Schnering, Angew. Chem. 104 (1992) 186.
[22] S.C. Miller, W.F. Love, Tables of Irreducible Representations of Space Groups and Co-Representation of Magnetic Space Groups, Pruett Press, Boulder, CO, 1967.
[23] M.-H. Whangbo, R. Hoffmann, R.B. Woodward, Proc. R. Soc. London Ser. A 366 (1979) 23.
[24] H.L. Skriver, O.K. Andersen, B. Johansson, Phys. Rev. Lett. 44 (1980) 1230.
[25] A. Savin, Second International Conference on Inorganic Chemistry, Stuttgart, Germany, 12–15 September 1993.
[26] F.R. Wagner, TopAn Program Package, Saarbrücken, 1998.
[27] F.R. Wagner, K. Stöwe, J. Solid State Chem. 157 (2001) 193.
[28] M. Grupe, W. Urland, J. Less-Common Met. 170 (1991) 271.
[29] S. Lee, B. Foran, J. Am. Chem. Soc. 11 (1994) 154.